Research paper

Performance Analysis and Modeling of a Variable Reluctance Speed Sensor for Turbomachinery Applications

A. H. Nejadmalayeri*, P. Yousefi, M. Safaei

Technical and Engineering Faculty, Imam Hossein Comprehensive University (IHU), Tehran, Iran.

Article Info	Abstract
	Background and Objectives: The speed sensor is one of the main components of the control and monitoring systems of rotational machines which is widely used in the aviation industry, railway, and automotive applications. Variable Reluctance Speed sensor (VRS) is a kind of magnetic sensor that has been traditionally employed for many different industrial measurements because of several well-known advantages, such as passive nature, non-contact operations, robustness, low cost, low sensitivity to dirt, and large-signal output. **Methods:** In this paper, a variable reluctance speed sensor is proposed. The design process of the proposed sensor is presented and both the magnetic and electrical models of this sensor are derived by assuming the effect of magnetomotive force caused by eddy current formed on the outer edge of the target gear at high frequencies. As a result, the proposed model can demonstrate the performance of the variable reluctance speed sensor at high frequencies very well. **Results:** The proposed VRS is designed and simulated using MATLAB and Ansys Maxwell software to verify the theoretical results is constructed and tested. **Conclusion:** In this paper, a variable reluctance speed sensor is proposed and studied. The magnetic and electrical models of the proposed sensor are derived and the output voltage equation has been calculated as a function of the air gap length. The proposed VR sensor is simulated using 2D Finite Element Analysis software to identify the main parameters that influence the sensor output and also to verify the accuracy of the model. According to the simulation results, the output waveform quality will be affected by parameters such as air gap length, target gear material, the self-inductance of the VR sensor, and the load component values. In terms of the electrical model, we were able to simulate the effect of load resistance and capacitance on the sensor output.

Introduction

The speed sensor is one of the main components of the control and monitoring systems of rotational machines which is widely used in the aviation industry, railway, and automotive applications [2]-[11]. For instance, for vibration-based damage detection of rotor blades in gas turbine engines, or for torsional vibration monitoring, it is necessary to measure instantaneous angular speed (IAS) as accurately as possible [12]-[19].

So far, several methods have been proposed for measuring IAS based on different kinds of sensing systems including Hall sensor-based, laser-based, optical encoders, capacitive and electromagnetic sensors, and potentiometric methods [20]-[25]. Variable Reluctance Speed sensor (VRS) is a kind of magnetic sensor that has been traditionally employed for many different industrial measurements because of several well-known advantages, such as passive nature, non-contact

operations, robustness, low cost, low sensitivity to dirt, and large-signal output. The main disadvantage of the VRS sensor is that the signal-to-noise ratio is very low at slow speeds and the output voltage depends on the target speed. In [26], a novel design and implementation of the VR sensors have been proposed which has resulted in an improvement in the speed measurement capabilities for turbomachinery. The proposed design provides an enhancement in output signal quality during the low and high-speed performance, and also during high-power operation. In addition, the new measuring system proposed in [26], has the capability for health monitoring of the engine bearings based on analysis of the differential output voltages from the two sensors. In [27], a numerical study has been performed on a VR sensor used for a coolant pump. In this research, a coupled circuit is introduced for calculating the induced voltage. The result of this study indicates that a sensor with a radially magnetized permanent magnet is more sensitive than C-shape. Also, a ferromagnetic yoke installation has the advantage of closing the magnetic circuit in order to increase the flux concentration within the circuit. All of these results will produce a higher output voltage. In [28], both the electrical and magnetic model of a VR sensor has been carried out and presented. In this paper, also the effect of load components on the output magnitude and resonant frequency of the output signal has been evaluated. In [29], [30], a speed measuring system is proposed based on the variable reluctance sensor in order to measure Instantaneous rotation speed and torsional vibration monitoring. In these papers, both the magnetic and electrical model of the system is proposed to evaluate the system quality. This model allows for simulating the behavior of the system, given the arbitrary shape and speed of the rotating target. All of the models presented in all of these articles have been simplified and the effect of magnetomotive force caused by eddy current formed on the outer edge of the target gear at high frequencies has not been considered. So, this model can't demonstrate the performance of the variable reluctance speed sensor at high frequencies very well. This paper is arranged as follows. In the first section, the basic theory of the variable reluctance speed sensor is described and both the magnetic and electrical equivalent circuits of the VR sensor are derived considering the effect of the eddy current that forms on the target gear. In the second section, 2D Finite Element Analysis (FEM) is used to model and simulate the output voltage generated by the sensor as a function of gear Instantaneous rotation speed. In the third section, an experimental setup is presented together with some experimental results confirming the results obtained from theory and simulation and finally, conclusions are drawn.

Modeling

As shown in Fig. 1, the structure of the VR sensor is made

of a permanent magnet that is responsible for generating magnetic flux, and a sensing coil that is wrapped around an iron core that acts as a probe. When a ferromagnetic target passes through the probe, loading the permanent magnet occur and causes variation of the magnetic flux density, which consequently crosses the sensing coil and according to faraday law, induces voltage on the sensing winding.
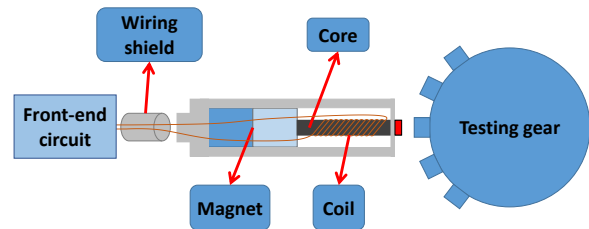

Fig. 1: Structure of variable reluctance speed sensor.

The system shown in Fig. 1 can be considered from two perspectives. In this section, both the magnetic and electrical model of the proposed VR sensor is derived. The magnetic part is composed of a magnet, ferrous iron core, and ferrous testing gear, and finally, the electrical section formed by the VRS coil, the wiring (usually a twin-axial cable), and the front-end electronics.

A. Magnetic Equivalent Circuit

The magnetic equivalent circuit of the system have shown in Fig. 1 can be derived using the usual approach exploiting the definition of the magnetic flux and applying the Ampere law to the identified flux line φ in Fig. 2(a), extending in the magnet for the section φ_m, and outside the magnet for the section φ_{lk}. Using the model shown in Fig. 2(a), the magnetic equivalent circuit can be derived as Fig. 2(b), in which R_m, R_{lk}, R_c, R_i and R_g are permanent magnet internal reluctance, leakage reluctance, iron core reluctance, sensor housing reluctance, and air gap reluctance respectively.
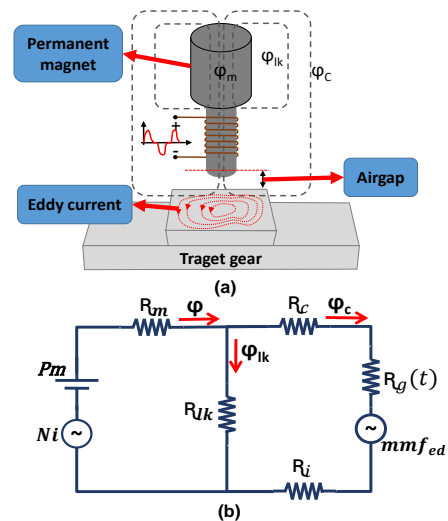

Fig. 2: Magnetic circuit derivation: (a) magnetic model, (b) magnetic circuit.

As shown in Fig. 2(a), air gap and sensor housing reluctances vary with the target gear motion. So, it can be considered as a function of time. Nevertheless, the value of R_{lk} is usually very large whereas R_i is so small, so they can be neglected in order to simplify the calculation. The flux in the magnetic circuit is generated by two magnetomotive forces (MMFs), a constant MMF relative to the permanent magnet, PM, in series with its internal R_m and the other given by MMF created by the sensing coil. By neglecting the current flowing in the sensing coil, this MMF can be ignored in calculations.

In Fig. 3, the result of the FEM analysis has been shown which indicates the accuracy of the magnetic equivalent circuit shown in Fig. 2(b).
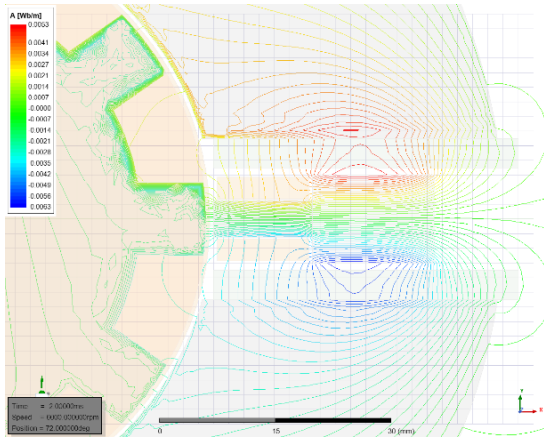

Fig. 3: FEM analysis of the target VR sensor.

The air gap reluctance can be defined by the following equation:

$$R_g = \frac{l_g(t)}{\mu_0 A_g} \tag{1}$$

where A_g is the equivalent surface of the gap area, $\mu 0$ is the air magnetic permeability, whereas $l_g(t)$ is the equivalent gap length as a function of the time. Therefore, as the target gear rotates, the air gap reluctance will be a time-dependent variable, which in turn causes a variable flux in the air gap. The air gap variation when the target gear rotates and considering 1-D geometry is shown in Fig. 4.
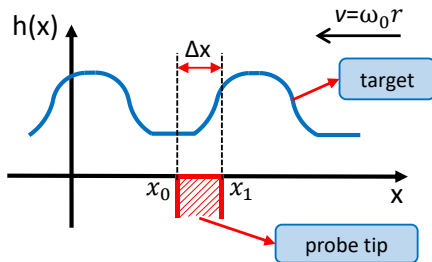

Fig. 4: Target gear and sensor tip profiles.

The target is supposed to move at the speed v, parallel to

axis x. According to Fig. 4, the average effective gap length can be defined as follows:

$$l_g(t) = \frac{1}{\Delta x} \int_{x_0}^{x_1} h(x - vt)\, dt \tag{2}$$

As explained previously, the leakage reluctance of VR sensors can be ignored to simplify calculations. So according to the equivalent magnetic circuit shown in Fig. 2(b), the magnetic flux can be calculated as follow:

$$MMF_t = (R_m + R_c + R_g(t) + R_i)\varphi \tag{3}$$

The MMF_t in (3) is the total magneto motive force that can be defined as follow:

$$MMF_t = Ni(t) + Pm + mmf_{ed} \tag{4}$$

where N is the number of turns in the sensing coil. By using the VR sensor in an electrical circuit, a current flow throws the sensing coil. So, this current makes the magnetomotive force $Ni(t)$ and also Pm is the MMF caused by the permanent magnet. MMF_{ed} in (4) is the magnetomotive force generated by eddy current formed on the outer edge of the target gear which is shown in Fig. 2(a). The magnetic flux equation can be written as follow:

$$\varphi(t) = \frac{Ni(t) + Pm + mmf_{ed}}{R_m + R_c + \frac{l_g(t)}{\mu_0 A_g} + R_i} \tag{5}$$

B. Electrical Equivalent Circuit

The equation which defines the magnetic flux has been calculated in the previous section. For calculating the induced voltage in the sensing coil of the VR sensor, the Faraday law can be used as follow:

$$V = -N \frac{d\phi(t)}{dt} \tag{6}$$

As shown in (5), the magnetic flux has been composed of three terms. The flux generated by sensing coil current, the flux generated by permanent magnet and finally the flux generated by target gear eddy current which generates harmonics on the output voltage of the sensor at high frequencies.

$$V_o(t) = V_{coil}(t) + V_{Pm}(t) + V_{mmfed}(t) \tag{7}$$

So, using (5) and (6), the induced voltages can be defined as follow:

$$V_{coil}(t) = -\frac{N^2}{R_t + \frac{l_g(t)}{\mu_0 A_g}} \frac{di(t)}{dt} + N^2 i(t) \frac{d}{dt} \frac{1}{R_t + \frac{l_g(t)}{\mu_0 A_g}} \tag{8}$$

$$V_{coil}(t) = -\frac{N^2}{R_t + \frac{l_g(t)}{\mu_0 A_g}} \frac{di(t)}{dt} + N^2 i(t) \frac{d}{dt} \frac{1}{R_t + \frac{l_g(t)}{\mu_0 A_g}} \tag{9}$$

$$V_{mmf_{ed}}(t) = -N.mmf_{ed} \frac{d}{dt} \frac{1}{R_t + \frac{l_g(t)}{\mu_0 A_g}} \tag{10}$$

where R_t is defined as follow:

$$R_t = R_m + R_c + R_i \tag{11}$$

The (8) that defines the voltage of the coil, is composed of two terms. According to the inductance voltage (12), the first term is the voltage that places on the self-inductance of the sensor. So, self-inductance can be defined as the (13).

$$V_{Lc} = L_c \frac{di(t)}{dt} \qquad (12)$$

$$L_c(t) = \frac{N^2}{R_t + \frac{l_g(t)}{\mu_0 A_g}} \qquad (13)$$

As shown in (13), the inductance value is a time-dependent variable because it depends on the air gap length.

The second term of (8), is opposing electromotive force respect to the one generated by the magnet that is shown by (14).

$$V_{op(t)} = N^2 i(t) \frac{d}{dt} \frac{1}{R_t + \frac{l_g(t)}{\mu_0 A_g}} \qquad (14)$$

$$V_{coil}(t) = L_c \frac{di(t)}{dt} + V_{op(t)} \qquad (15)$$

So, we have (16) for the output voltage:

$$V_o(t) = V_{Lc}(t) + V(t) \qquad (16)$$

where:

$$V(t) = V_{op}(t) + V_{Pm}(t) + V_{mmfed}(t) \qquad (17)$$

By assuming R_{coil} as the parasitic resistance of the sensing coil and according to the (16) and (17) that defines the output voltage and the voltage induced in the coil, the electrical model of the VR sensor can be derived as Fig. 5. The load component considered at the output of the sensor is used to adjust the amplitude of the output waveform for a range of frequencies. The variation of the output pulse for a different amount of the load impedance is shown in Fig. 6.
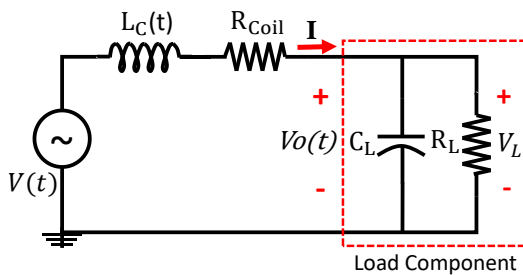

Fig. 5: Equivalent electrical circuit of the VR sensor.

The sensor current, can be calculated by solving the differential equation below:

$$L_c(t) \frac{dI(t)}{dt} + R_{Coil} I(t) + Z_L I(t) = V(t) \qquad (18)$$

It is obvious that (18) is not an ordinary differential equation with constant parameters, so it has to be solved numerically.

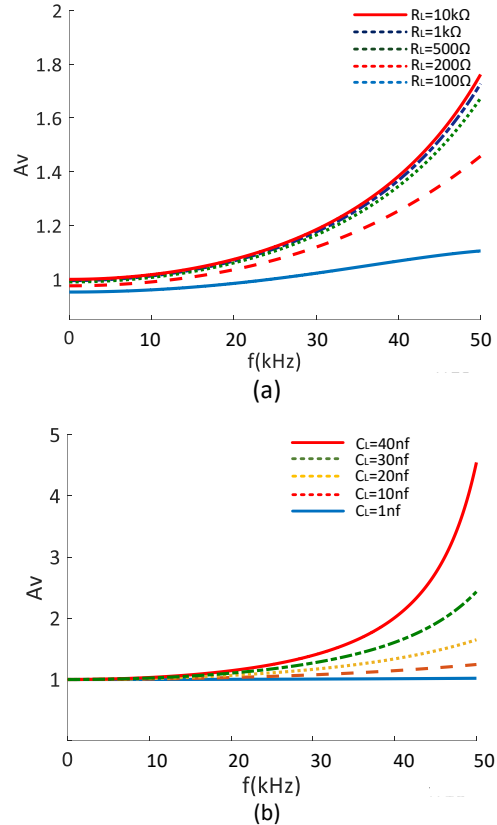
Fig. 6: The output voltage changes for different frequencies, (a) CL=1nf; (b) RL=10KΩ.

Design and Simulation of the proposed sensor

In this section, the design process of the proposed VR sensor is shown and then the simulations are performed according to the design results. As shown in Fig. 7, the design process of the VRS sensor is an iterative process. At the first step of the design process, the magnet and pole piece are selected as Table 1. By assuming *V(t)*=5v for the output voltage, the design process continue until the desired value for V(t) is reached.

The 2D Finite Element Analysis (FEM) is used for the simulation of the output voltage generated by the sensor. The distribution of the magnetic flux during target gear rotation is shown in Fig. 8 for two different states of assuming and regardless of the target gear eddy current. As previously explained, the magnetic flux produced by the target gear eddy current causes harmonics and makes distortion on the sensor output voltage.

Table 1: VR Sensor simulation parameters

	Material	Electromagnetic Properties	Dimensions (mm) length×diameter
Magnet	NeFeB	H_C = 1034507 A/m, μ_r = 1.05	8×4
Pole Piece	Ferrite	Linear B-H Curve	5×4

156

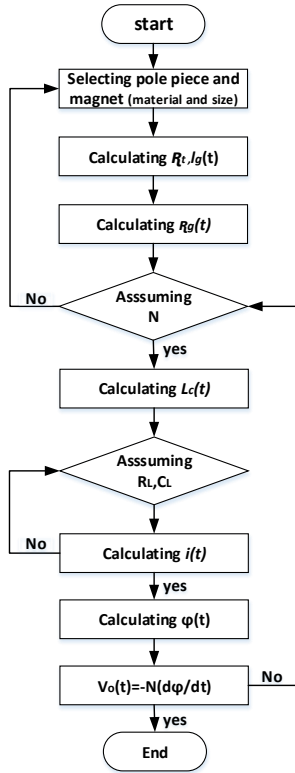*J. Electr. Comput. Eng. Innovations, 11(1): 153-160, 2023*

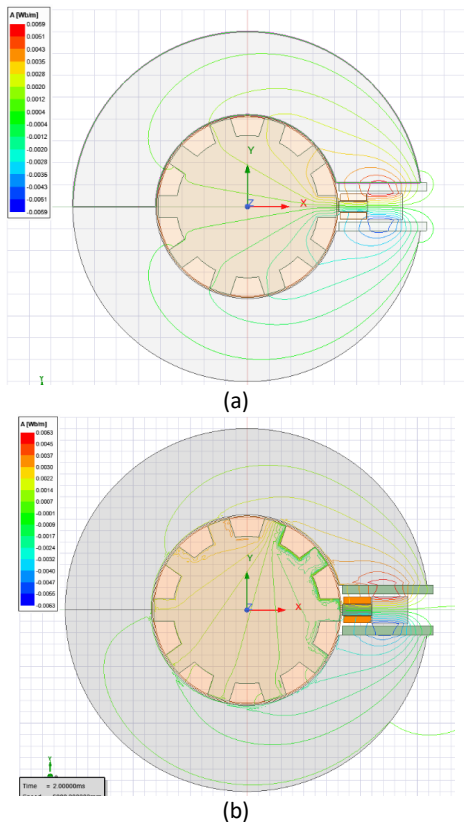Fig. 7: The design process of the proposed VRS sensor.

(a)

(b)

Fig. 8: Target simulation, (a) magnetic flux by Ignoring eddy current effect. (b) magnetic flux by considering eddy current effect.

So, in order to obtain the sensor coil voltage induced by the target gear eddy current, the simulation is performed in two ways, once by ignoring the effect of the flux generated by the target gear eddy current and then by considering the eddy current effect. The output voltage for both of the simulation states is shown in Fig. 9(a).

As shown in Fig. 9, the flux caused by the eddy current generated on the outer edge of the target gear makes distortion on the voltage induced in the sensor coil. The voltage caused by the eddy current is shown in Fig. 9(b).
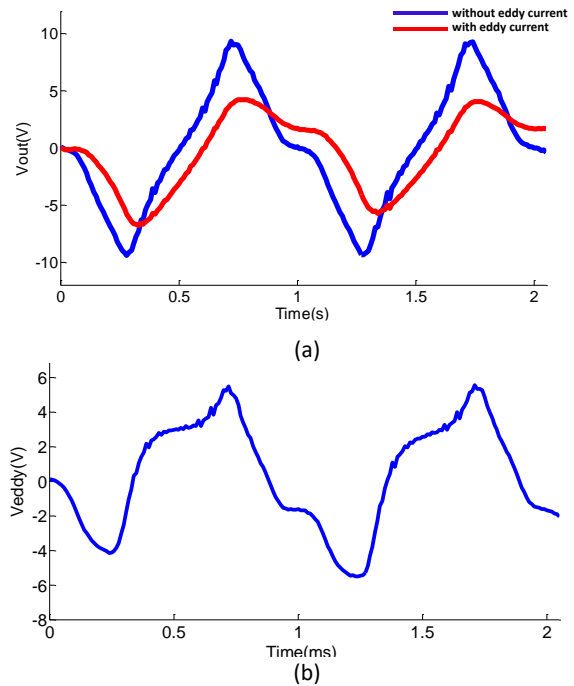

(a)

(b)

Fig. 9: Simulation results, (a) The output voltage of the VR speed sensor for 6000RPM (b) The voltage induced in the coil by the eddy current flux.

This voltage waveform is the result of the difference between the two waveforms shown in Fig. 9(a). A comparison of the two waveforms shown in Fig. 9(a) and Fig. 9(b) indicates that the flux generated by the target gear eddy current, acts in the opposite direction of the main flux and it weakens the main magnetic field. So, as shown in Fig. 2(b), it can be modeled as a magnetomotive force (MMF$_{ed}$) in the magnetic circuit. The value of the MMF$_{ed}$ is proportional to the rotation frequency of the target gear. So, the higher instantaneous rotational speed, the greater distortion of the output waveform. The sensor output voltage for two different speeds is shown in Fig .10

The self-inductance variation is shown in Fig. 11 for the target gear. As shown in Fig. 11 and according to (13), the self-inductance varies with air gap length variations.

The amount of the induced voltage due to the MMF$_{ed}$ is related directly to the magnetic permeability coefficient of the target gear material. As the magnetic permeability increases, the voltage induced by MMF$_{ed}$ which is shown

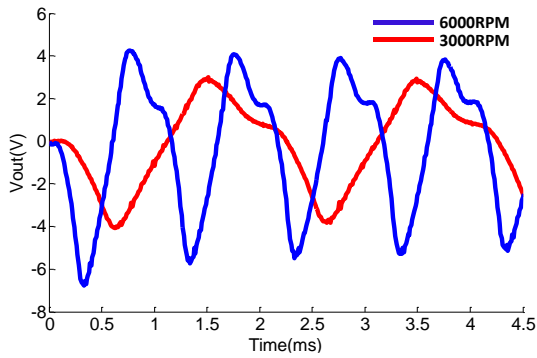in Fig. 9(b) decreases and the sensor output waveform will be more appropriate.

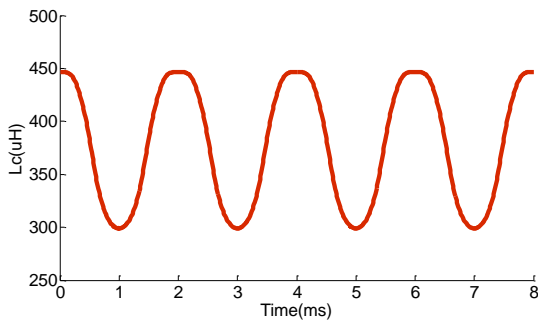Fig. 10: The sensor output voltage for two different speed.

Fig. 11: VR sensor self-inductance variations in 3000RPM.

In order to show this issue, simulation has been performed for three different types of the target gear material which is shown in Table 2.

Table 2: Different target gear materials

Material	Relative Permeability	Metal Conductivity(S/m)
Iron	4000	10300000
Aluminum	1.000021	38000000
Steel	1	1100000

As shown in Fig. 12, the iron target gear with the highest magnetic permeability coefficient compared to the aluminum and steel materials has the best output result.
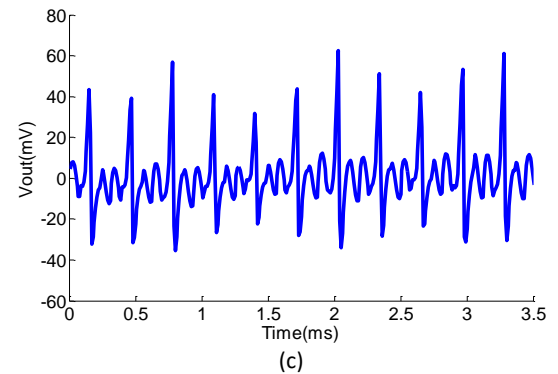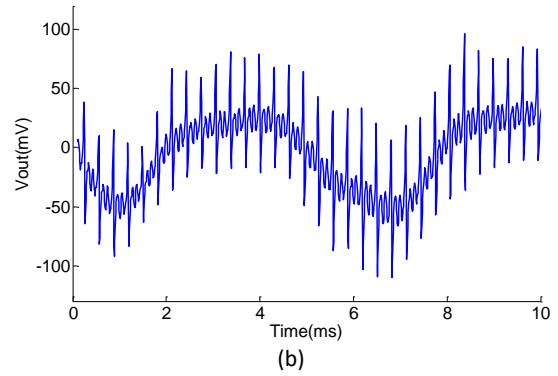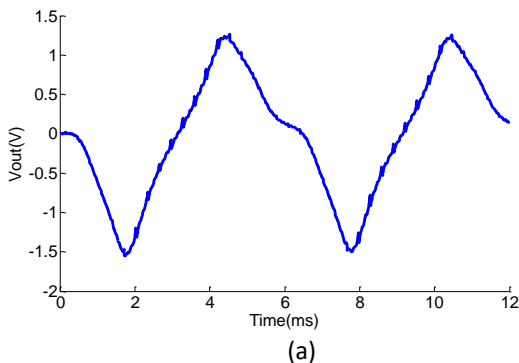

(a)

(b)

(c)

Fig. 12: The sensor output voltage for different target gear materials (a) Iron, (b) Aluminum, (c) Steel.

Experimental Results

An experimental test is used to validate the magnetic model derived and presented in previous sections. As shown in Fig. 13, the test system consists of a variable speed motor and, a target gear with 10 teeth and a VR sensor with the characteristics shown in Table 1.
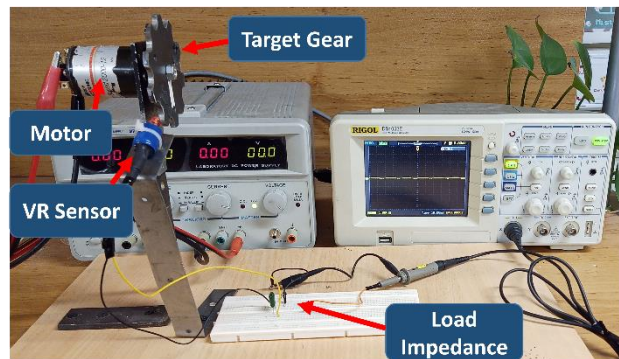

Fig. 13: Experimental set-up used for the tests.

The sensor output signal was acquired with a digital oscilloscope (RIGOL DS1052E) and The VR sensor is loaded by a large impedance as shown in figure5. The test is performed and the experimental result of the test is shown in Fig. 14.

As explained at previous sections, the output waveform of the VR sensor is always a function of the target gear geometry, material and airgap length. The output voltage waveform of the VR sensor for an iron

target gear is shown in Fig. 14(a). According to the magnetic circuit shown in Fig. 2(b), and the high relative permeability of iron, most of the magnetomotive force (MMF_{ed}) generated in this mode is related to the sensor magnet and MMF_{ed} is so weaker than the total MMF. So, in this case, the voltage waveform has lower harmonics and is very similar to the target gear geometry.

The second test has been performed using an aluminum target gear as shown in Fig. 14(b). As shown in Fig. 2(b) and due to the low value of the relative permeability of aluminum, the voltage waveform is distorted. Therefore, to use this sensor for applications such as vibration monitoring or blade tip timing in turbomachinery, using complex electronic circuits to eliminate the sensor output waveform is necessary.

The amplitude of the output voltage waveform can be adjusted according to Fig. 6 by changing the output load impedance. So that the voltage amplitude changes at different frequencies do not deviate from the linear state.

The comparison of the experimental output waveform of the proposed VR sensor by the simulation results that shown in Fig. 12(a) and Fig. 12(b), ensures the accuracy of the modeling performed.
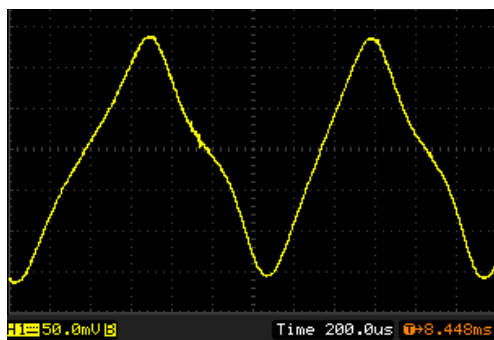
(a)
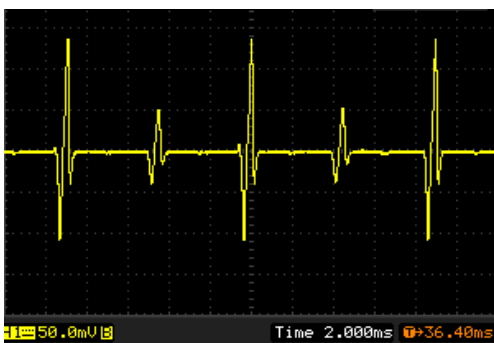
(b)

Fig. 14: Experimental test result of the proposed VR sensor (a)Iron target gear (b)Aluminum target gear.

Conclusions

In this paper, a variable reluctance speed sensor is proposed and studied. The magnetic and electrical models of the proposed sensor are derived and the output voltage equation has been calculated as a function of the air gap length. The proposed VR sensor is simulated using 2D Finite Element Analysis software to identify the main parameters that influence the sensor output and also to verify the accuracy of the model. According to the simulation results, the output waveform quality will be affected by parameters such as air gap length, target gear material, the self-inductance of the VR sensor, and the load component values. In terms of the electrical model, we were able to simulate the effect of load resistance and capacitance on the sensor output.

Author Contributions

Acknowledgment

Conflict of Interest

The authors declare no potential conflict of interest regarding the publication of this work. In addition, the ethical issues including plagiarism, informed consent, misconduct, data fabrication and, or falsification, double publication and, or submission, and redundancy have been completely witnessed by the authors.

Abbreviations

VRS	Variable Reluctance Sensor
IAS	Instantaneous Angular Speed
FEM	Finite Element
MMF	Magneto Motive Forces

References

[1] S. Merhav, Aerospace sensor systems and applications. Springer Science & Business Media, 1998.

[2] F. Chaaban, T. Birch, D. Howe, P. Mellor, "Topologies for a permanent magnet generator/speed sensor for the ABS on railway freight vehicles," in Proc. 1991 Fifth International Conference on Electrical Machines and Drives (Conf. Publ. No. 341), IET: 31-35, 1991.

[3] B. Wang, "Design of teaching platform for ABS wheel speed sensor," J. Phys. Conf. Ser., 2187(1): IOP Publishing: 012004, 2022.

[4] R. Przysowa, E. Rokicki, "Inductive sensors for blade tip-timing in gas turbines," J. KONBiN, 36(1): 147, 2015.

[5] D. Heller, I. Sever, C. Schwingshackl, "A method for multi-harmonic vibration analysis of turbomachinery blades using Blade Tip-Timing and clearance sensor waveforms and optimization techniques," Mech. Syst. Sig. Process., 142: 106741, 2020.

[6] A. Vercoutter, M. Berthillier, A. Talon, B. Burgardt, J. Lardies, "Estimation of turbomachinery blade vibrations from tip-timing data," in Proc. 10th International Conference on Vibrations in Rotating Machinery: 11-13, 2012.

[7] Y. S. Didosyan, H. Hauser, H. Wolfmayr, J. Nicolics, P. Fulmek, "Magneto-optical rotational speed sensor," Sens. Actuators, A, 106(1-3): 168-171, 2003.

[8] P. Procházka, F. Vaněk, "New methods of noncontact sensing of blade vibrations and deflections in turbomachinery," IEEE Trans. Instrum. Meas., 63(6): 1583-1592, 2013.

[9] T. Achour, M. Pietrzak-David, "Service continuity of an IM distributed railway traction with a speed sensor fault," in Proc. the

2011 14th European Conference on Power Electronics and Applications, : 1-8, 2011.

[10] Y. Maniwa, S. Kitamura, K. Aoyama, M. Matsuyama, "Turbomachinery control by CENTUM VP," Yokogawa Technical Report-English Edition-, 45: 47, 2008.

[11] M. Dowell, G. Sylvester, "Turbomachinery prognostics and health management via eddy current sensing: current developments," in Proc. 1999 IEEE Aerospace Conference (Cat. No. 99TH8403), 3: 1-9, 1999.

[12] Y. Li, F. Gu, G. Harris, A. Ball, N. Bennett, K. Travis, "The measurement of instantaneous angular speed," Mech. Syst. Sig. Process., 19(4): 786-805, 2005.

[13] S. Madhavan, R. Jain, C. Sujatha, A. Sekhar, "Vibration based damage detection of rotor blades in a gas turbine engine," Eng. Fail. Anal., 46: 26-39, 2014.

[14] A. Darpe, K. Gupta, A. Chawla, "Coupled bending, longitudinal and torsional vibrations of a cracked rotor," J. Sound Vib., 269(1-2): 33-60, 2004.

[15] S. W. Doebling, C. R. Farrar, M. B. Prime, "A summary review of vibration-based damage identification methods," Shock Vib. Digest, 30(2): 91-105, 1998.

[16] L. Doliński, M. Krawczuk, "Damage detection in turbine wind blades by vibration based methods," J. Phys. Conf. Ser., 181(1): IOP Publishing: 012086, 2009.

[17] C. Liu, D. Jiang, "Improved blade tip timing in blade vibration monitoring with torsional vibration of the rotor," J. Phys. Conf. Ser., 364(1): IOP Publishing: 012136, 2012.

[18] L. Naldi, M. Golebiowski, "New approach to torsional vibration monitoring," in Proc. the 40th Turbomachinery Symposium, Texas A&M University. Turbomachinery Laboratories, 2011.

[19] F. L. M. Dos Santos, B. Peeters, H. Van Der Auweraer, L. Góes, W. Desmet, "Vibration-based damage detection for a composite helicopter main rotor blade," Case Stud. Mech. Syst. Sig. Process., 3: 22-27, 2016.

[20] S. Kaul, R. Koul, C. Bhat, I. Kaul, A. Tickoo, "Use of alook-up'table improves the accuracy of a low-cost resolver-based absolute shaft encoder," Meas. Sci. Technol. 8(3): 329, 1997.

[21] X. Li, G. C. Meijer, "A novel low-cost noncontact resistive potentiometric sensor for the measurement of low speeds," IEEE Trans. Instrum. Meas., 47(3): 776-781, 1998.

[22] T. Fabian, G. Brasseur, "A robust capacitive angular speed sensor," IEEE Trans. Instrum. Meas., 47(1): 280-284, 1998.

[23] R. M. Kennel, "Encoders for simultaneous sensing of position and speed in electrical drives with digital control," IEEE Trans. Ind. Appl. 43(6): 1572-1577, 2007.

[24] M. Nandakumar, S. Ramalingam, S. Nallusamy, S. Srinivasarangan Rangarajan, "Hall-sensor-based position detection for quick reversal of speed control in a BLDC motor drive system for industrial applications," Electronics, 9(7): 1149, 2020.

[25] L. Avanesov Yuriy, N. Bukanova Ayna, S. Voronov Alexander, I. Evstifeev Michail, "Optimization of design parameters for depth electromagnetic speed sensor," J. Sci. Tech. Inf. Technol., Mech. Opt., 113(1): 140-146, 2018.

[26] J. J. Costello, A. C. Pickard, "A novel speed measurement system for turbomachinery," IEEE sens. Lett., 2(4): 1-4, 2018.

[27] H. Huh, J. S. Park, S. Choi, K. B. Park, S. Q. Zee, "Numerical research on new variable reluctance sensor with fixed permanent magnet for SMART main coolant pump," in Proc. the Korean Nuclear Society Conference, Korean Nuclear Society: 1045-1046, 2005.

[28] R. A. Croce Jr, I. Giterman, "Development of the Electrical and Magnetic Model of Variable Reluctance Speed Sensors."

[29] T. Addabbo et al., "Instantaneous rotation speed measurement system based on variable reluctance sensors for torsional vibration monitoring," IEEE Trans. Instrum. Meas., 68(7): 2363-2373, 2018.

[30] T. Addabbo et al., "Instantaneous rotation speed measurement system based on variable reluctance sensors: Model and analysis of performance," in Proc. 2018 IEEE Sensors Applications Symposium (SAS): 1-6, 2018.

Biographies

Amir Hossein Nejadmalayeri received his B.Sc. degree in Electrical Engineering from Shahid Bahonar University, Kerman, Iran, in 2018 and his M.Sc. degree in Electrical Engineering from Malek-Ashtar University of Technology, Tehran, Iran, in 2021. His research interests include design, modeling of power converters, and pulsed power systems.

- Email Address: malayeri@ihu.ac.ir
- ORCID: 0000-0002-8506-5959
- Web of Science Researcher ID: GLV-1497-2022
- Scopus Author ID: NA
- Homepage: NA

Meysam Safaei received his B.Sc. degree in electrical engineering from University of Eyvanekey, Teharn, Iran, in 2011 and his M.Sc. degree in artificial intelligence and robotics engineering from Malek-Ashtar University of Technology, Tehran, Iran, in 2022. His research interests include artificial intelligence and IOT.

- Email Address: safaei@ihu.ac.ir
- ORCID: 0000-0002-4544-4284
- Web of Science Researcher ID: GLV-2737-2022
- Scopus Author ID: NA
- Homepage: NA

160

J. Electr. Comput. Eng. Innovations, 11(1): 153-160, 2023